

Differential Bio-Optoelectronic Gating of Semiconducting Carbon Nanotubes by Varying the Covalent Attachment Residue of a Green Fluorescent Protein

Rebecca E. A. Gwyther, Nikita P. Nekrasov, Aleksei V. Emelianov, Albert G. Nasibulin, Krithika Ramakrishnan, Ivan Bobrinetskiy,* and D. Dafydd Jones*

Integrating photoactive proteins with synthetic nanomaterials holds great promise in developing optoelectronic devices whereby light, captured by an antenna protein, is converted to a modulated electrical response. The protein–nanomaterial interface is critical to defining optoelectronic properties; successful integration of bionanohybrids requires control over protein attachment site and a detailed understanding of its impact on device performance. Here, the first single-walled carbon nanotube (SWCNT) bio-optoelectronic transistor enabled by the site-specific direct interfacing with a green fluorescent protein (GFP) via genetically encoded phenyl azide photochemistry is reported. The electrical behavior of individual semiconducting SWCNTs depends on the protein residue coupling site and provides the basis to design eco-friendly phototransistors and optoelectronic memory. Attachment at one GFP residue proximal to the chromophore produces a wavelength-specific phototransistor. The bio-transistor can be switched off in less than 38 s with responsivity up to $7 \times 10^3 \text{ A W}^{-1}$ at 470 nm. Attachment via a second residue distal to the chromophore generates optoelectronic memory that show rapid and reproducible conductivity switching with up to 15-fold modulation that is restored on the application of a gate voltage. Therefore, photoactive proteins, especially GFP, can be realized as a key material for novel single-molecule electronic and photonic devices.

1. Introduction

Optoelectronic devices based on interfacing biomolecules with existing molecular electronic materials have generated great interest both in terms of being eco-friendly, low-cost next-generation electronics based on novel computing principles.^[1,2] A key facet for any successful implementation is communication between the molecular entities, so events in one (e.g., biomolecular function) alter the other (e.g., conductance).^[3] With regards to bio-based optoelectronic devices, fluorescent proteins^[4,5] can act as the light-responsive element that transduces events through to a nanocarbon conductance base, such as single-walled carbon nanotubes (SWCNTs) and graphene. SWCNTs' conductance and optical properties make them particularly useful for generating active bionanohybrid systems, especially as their inherent properties can be altered through chemical

R. E. A. Gwyther, K. Ramakrishnan, D. D. Jones
Molecular Biosciences Division
School of Biosciences
Sir Martin Evans Building
Cardiff University
Museum Avenue
Cardiff CF10 3AX, UK
E-mail: jonesdd@cardiff.ac.uk


N. P. Nekrasov, A. V. Emelianov, I. Bobrinetskiy
Center for Probe Microscopy and Nanotechnology
National Research University of Electronic Technology
Moscow, Zelenograd 124498, Russia
E-mail: bobrinet@biosense.rs, bobrinet@gmail.com

A. V. Emelianov
Division of Solid State Physics
P.N. Lebedev Physical Institute of the Russian Academy of Sciences
Moscow 119991, Russia

A. G. Nasibulin
Center for Photonics and Quantum Materials
Skolkovo Institute of Science and Technology
Nobel Street 3, Moscow 143026, Russia

A. G. Nasibulin
Department of Chemistry and Materials Science
Aalto University
Espoo 02150, Finland

I. Bobrinetskiy
BioSense Institute
Research and Development Institute for Information Technologies
in Biosystems
University of Novi Sad
Novi Sad 21000, Serbia

 The ORCID identification number(s) for the author(s) of this article can be found under <https://doi.org/10.1002/adfm.202112374>.

© 2022 The Authors. Advanced Functional Materials published by Wiley-VCH GmbH. This is an open access article under the terms of the Creative Commons Attribution License, which permits use, distribution and reproduction in any medium, provided the original work is properly cited.

DOI: 10.1002/adfm.202112374

modifications,^[6–8] including with proteins.^[9–11] Their cylindrical structure makes them more compatible with protein interfacing compared with graphene, whose large hydrophobic area can induce protein unfolding and thus loss of protein function.^[12] Here, we focus on how optically active proteins can be used to modulate conductance across an individual SWCNT transistor.

Nature has created a myriad of proteins capable of interacting with and responding to light at various wavelengths across the UV–visible region of the electromagnetic spectrum.^[13–15] In the case of an optoelectronic system, electronic excitation can be coupled to secondary events such as conductance.^[16–19] Fluorescent proteins (FPs)^[4,20] such as green fluorescent protein (GFP)^[5] are finding uses outside of their classical cell imaging role as components in molecular electronics such as light-harvesting and energy transfer,^[21] light-emitting diodes (LEDs),^[22] solid-state protein lasers,^[23] and optically gated transistors.^[24] Electronic excitation is coupled to charge transfer and light emission as part of the fluorescence photocycle.^[25] FPs have advantages over small organic molecule components as the protein shell encases the chromophore, protecting it from the external environment and helping to tune the electronic properties of the chromophore, including through the formation of long-range charge transfer pathways.^[26] The dimensions of FPs ($\approx 3 \text{ nm} \times 5 \text{ nm}$) match well with nanocarbon materials such as SWCNTs (diameter 1–2 nm; **Figure 1a**).

By coupling FPs to CNTs, there is a possibility of exploiting emergent single fluorescent protein molecule function in the context of novel electronic devices through tuning optical and electrical properties.^[27–30] Recently, a number of papers have demonstrated the enhancement of photocurrent response of graphene^[31] or carbon nanotube transistors^[32] modified by photosensitive proteins. For example, GFP covalent attachment via diazonium salts was used to develop the wavelength selective photodetector based on a graphene field-effect transistor (FET).^[33] However, most of these approaches do not allow the attachment site to be defined and systematically varied

to optimize and/or alter the protein-dependent conductance characteristics.

Ideally, the protein should be attached to the carbon nanotube (CNT) at a designed residue to generate a defined, stable, intimate, and homogenous interface with optimal transduction between the two (**Figure 1b**). Furthermore, the ability to change the interface configuration through changing the protein interfacing residue can lead to different characteristics through, for example, changing access to the charge transfer pathways in the protein.^[28,30] Most approaches using conjugation chemistry based on primary amine (lysine) chemistry do not allow defined attachment. For example, in the GFP variant we use here, termed superfolder GFP (sfGFP),^[34] there are 19 lysine residues spread across the protein's structure (**Figure 1b**). We have recently shown that proteins, including GFP, can be site-specifically covalently attached to graphene^[35] and CNTs^[30] using genetically encoded phenyl azide photochemistry (**Figure 1c**); phenyl azide photochemistry makes generating bionanohybrids easier and more precise as the new abiotic chemistry is incorporated site-specifically at one single location by design.^[36,37] Furthermore, the phenyl azide moiety can easily be moved to different residues in a protein, changing the nature of the protein–CNT interaction and thus the transduction process. The attachment mechanism is shown in **Figure 1c** and involves irradiation with UV light, which converts the phenyl azide into a nitrene radical^[38] that can then covalently link to the electron-rich region of a CNT.^[30]

In this work, we demonstrate the use of SWCNT FET photochemically modified with two different phenyl azide containing variants of sfGFP (**Figure 1a**) for the development of optoelectronic devices. Changing the protein's interfacing residue alters the CNT device properties. We demonstrate that the light-dependent electron-donating nature of GFP decreases the conductivity of p-type semiconducting SWCNT (scSWCNT) by circa an order of magnitude upon light illumination close to the peak absorbance wavelength for GFP. To our knowledge, this is the first-time individual carbon nanotube-based transistors

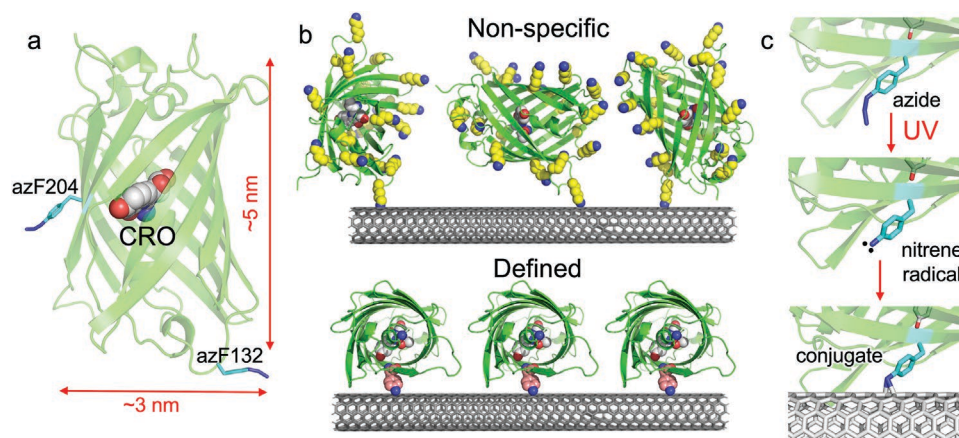


Figure 1. Attachment of GFP to CNTs. a) The structure of the superfolder version of GFP^[34] (PDB 2B3P) mutated in silico to contain *p*-azido-L-phenylalanine (azF) at residues 132 or 204 (cyan and shown as sticks). The chromophore (CRO) is shown as grey spheres with relative dimensions shown in red. b) Schematic outline illustrating non-specific attachment of GFP by, for example, primary amine chemistry via lysine residues (shown as yellow spheres) and defined, single-site attachment via genetically encoded phenyl azide photochemistry (shown as pink spheres). c) CNT attachment using phenyl azide photochemistry. Illumination with UV light (305 nm) generates a nitrene radical that can covalently crosslink to the electron-rich CNT across a C=C bond.

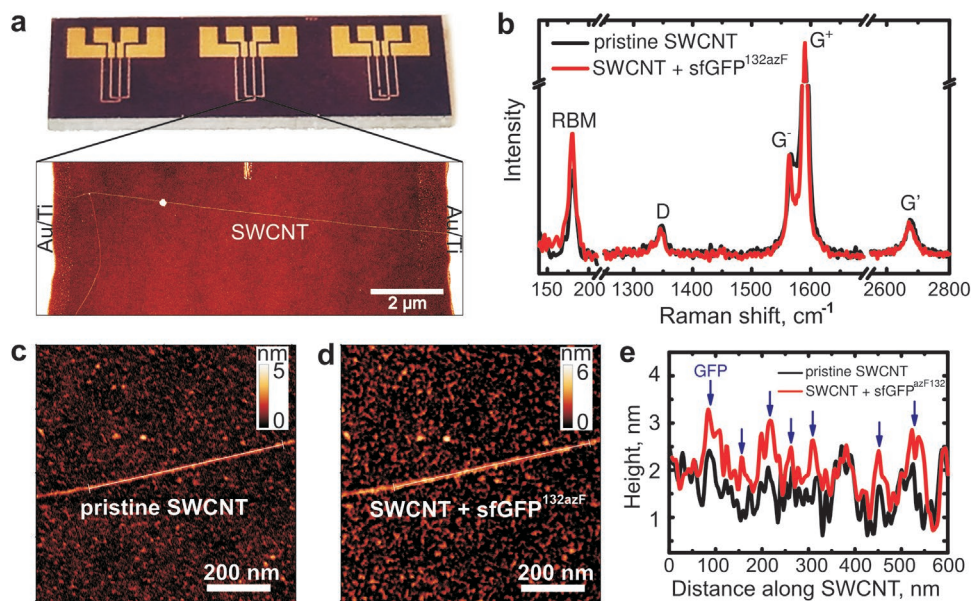


Figure 2. Characterization of SWCNT channel during sfGFP attachment. a) Optical image of a typical chip used here (top), including an AFM image of the layout of the electrodes of the SWCNT FET device (bottom). b) Raman spectra of SWCNT taken with an excitation wavelength of 532 nm and spot size of 1 μm for untreated, pristine SWCNT (black) and after attachment of sfGFP^{132azF} (red). c) AFM image of an individual SWCNT (c) before and (d) after sfGFP^{132azF} attachment. e) Cross-section along the nanotube axis before (black) and after (red) sfGFP^{132azF} attachment. The linear section measured is indicated by white lines in (c) and (d), respectively. Likely attachment sites of sfGFP^{132azF} are shown as blue arrows.

have been photochemically modified with a protein and shown direct orientation-specific effects on conductance modulation.

2. Results and Discussion

2.1. Site-specific Photochemical GFP Attachment onto Individual SWCNT FETs

We have previously engineered sfGFP to contain the non-natural amino acid *p*-azido-L-phenylalanine (azF) at either residue 132 (sfGFP^{132azF}) or 204 (sfGFP^{204azF}) (Figure 1a).^[39] When free in solution, both sfGFP^{132azF} and sfGFP^{204azF} have characteristic absorbance spectra similar to unmutated, wild-type sfGFP, with λ_{max} at ≈ 490 nm^[39] (Figure S1, Supporting Information). The sfGFP^{132azF} variant is termed the long axis variant as the SWCNT attachment residue is positioned at the end of the β -barrel GFP structure distal from the functional center, the chromophore (Figure 1a); the estimated distance between the chromophore and azF is ≈ 2.5 nm. The sfGFP^{204azF} variant is termed the short axis variant as residue 204 is positioned on the side of the β -barrel close to chromophore (Figure 1a), resulting in a shorter distance between the chromophore and the attachment site (≈ 1 nm). Here, we attached the sfGFP variants to SWCNT transistors using the UV irradiation approach described previously via the mechanism outlined in Figure 1c.^[30,35]

The working area of a FET device containing an individual SWCNT channel (Figure 2a) was immersed in a low protein concentration (100 nM) buffered solution so that proteins would be relatively well spaced on the SWCNT sidewall. Raman spectrum for an individual pristine SWCNT channel is shown in Figure 2b. Analysis of the observed E33 optical transition revealed that the SWCNT corresponds to a (11, 10) scSWCNT

with a diameter of 1.42 nm.^[40] Raman spectrum for scSWCNT after modification with azF containing protein (Figure 2b) shows almost no change in the intensities of the D and G bands in line with previous observations for low occurrence bond disruption events due to low-frequency protein photochemical attachment (estimated to be $\approx 0.01\%$ C=C bond disruption events based on the distribution of protein on SWCNT).^[35] G⁻ and G⁺ bands have minor changes after protein attachment (see Table S1, Supporting Information). We observed a small G' band shift to lower wavenumbers (Figure S2 and Table S1, Supporting Information), which indicates weak n-type doping of carbon nanotube on protein attachment.^[41] The absence of major changes in Raman spectra, normally associated with large-scale oxidation,^[42,43] is not unexpected and is evidence of the low protein coverage on the SWCNT we aimed to achieve.

Atomic force microscopy (AFM) was used to assess the attachment of protein molecules to the SWCNT (Figure 2c,d). Image analysis of SWCNTs modified with sfGFP revealed periodic height increases of ≈ 1.5 nm compared to the pristine SWCNTs prior to modification indicating successful attachment of protein (Figures 2c-e and S3, Supporting information).^[30] While the height changes are lower than expected based on the protein crystal structure dimensions, this is in line with previous observations for sfGFP and proteins in general whereby AFM can underestimate heights of soft molecules like proteins together with protein attachment occurring around the nanotube diameter rather than solely at the apex.^[30,44,45] Moreover, the pristine SWCNT average diameter is estimated to be 1.6 ± 0.2 nm providing a larger surface area for GFP attachment compared to previously published thinner nanotubes.^[28,30] The small amount of baseline variation observed for the pristine SWCNT is likely due to an uneven substrate surface. The presence of prominent peaks above the pristine SWCNT heights

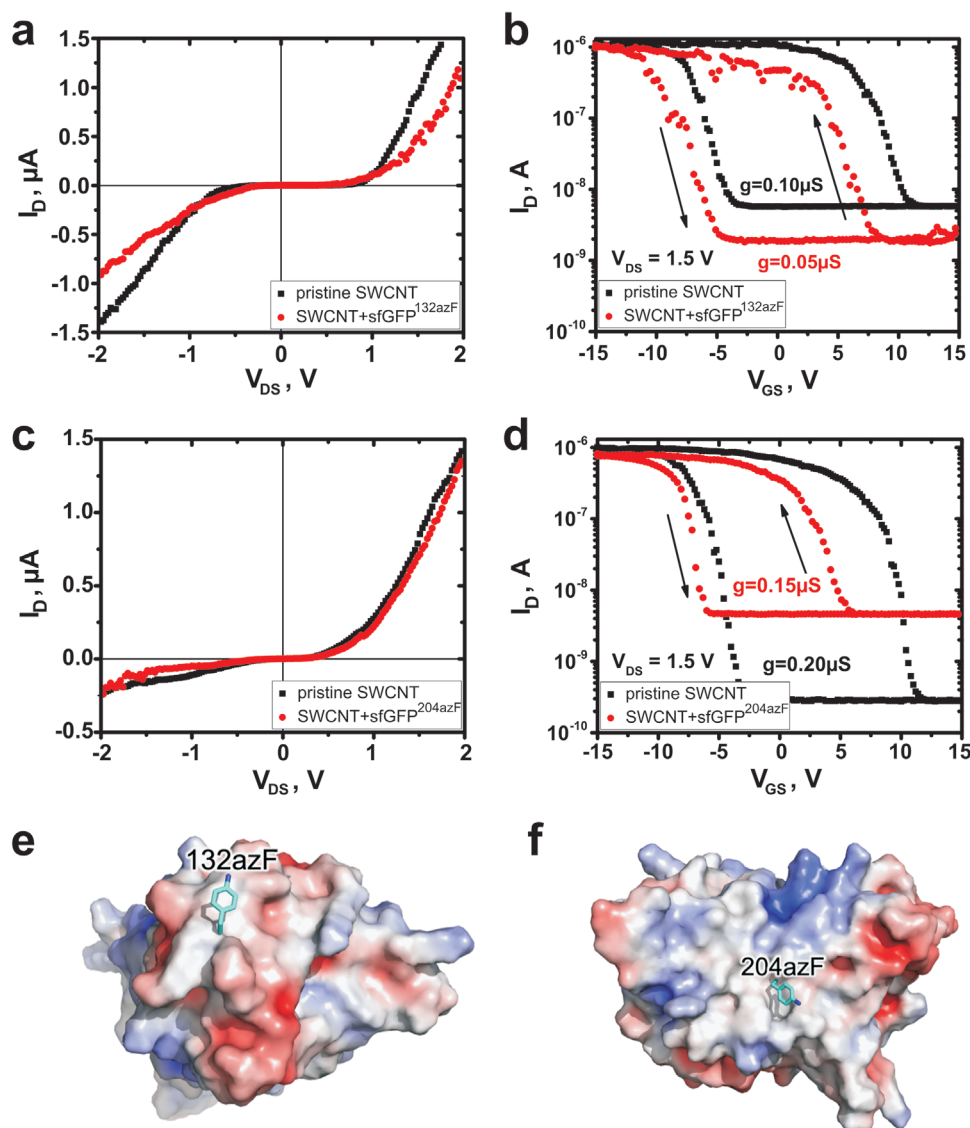


Figure 3. Changes in electrical properties after protein attachment to scSWCNT. Output and transfer current-voltage characteristics of SWCNT-FETs before and after azF containing GFP attachment to SWCNTs for sfGFP^{132azF} (a, b) and sfGFP^{204azF} (c, d). Electrostatic surface profile of sfGFP from the perspective of 132azF (e) and 204azF (f) residue sites (colored cyan). The color change from blue to red at (e, f) corresponds to a shift from positive to negative charges while white is neutral. In each case, protein attachment was performed with 100 nM of the GFP variant. Control CVC curves SWCNTs treated with wild-type GFP (no phenyl azide group) are shown in Figure S5 (Supporting Information).

are provide strong evidence for the presence of protein on the nanotube (Figure 2d-e). The increased heights on protein attachment observed in the lateral measurements are confirmed by the cross-sectional analysis presented in Figures S3 and S4 (Supporting Information).

From analysis of the AFM data, we estimate there is *circa* one sfGFP protein per 60–80 nm of SWCNT length (Figure 2e), which is approximately 120–170 proteins in the channel. We have observed similar changes in AFM and Raman characteristics of the SWCNT modified by sfGFP^{204azF} using the same method described above but using a higher protein concentration during attachment (Figure S4 and Table S2, Supporting Information). As expected, the protein density, in this case, was higher, with one protein per 40–50 nm of SWCNT length. The higher protein density could be the reason for the

more prominent changes observed in the Raman spectrum for sfGFP^{204azF} due to increased disruption to the SWCNT sp² bond network on covalent attachment of the protein.

Prior to protein attachment, the current-voltage characteristics (CVCs) of the SWCNTs showed typical p-doped semiconducting behavior with a Schottky barrier formed near the electrodes (Figure 3). A current I_{on}/I_{off} ratio of about $10^2 - 10^3$ indicates a small energy gap in the nanotubes. Protein attachment residue should have a major impact on the modulation of electrical properties of SWCNTs by sampling different electrostatic surfaces and distances from the chromophore. After sfGFP attachment, CVCs show a decrease in conductivity, which was particularly pronounced for sfGFP^{132azF} (Figure 3a). Increase in the I_{on}/I_{off} ratio (Figure 3b) can be associated with the energy bandgap broadening in the nanotube due to the

electrostatic nature of the protein surface around residue 132 (Figure 3e). In addition, we observe the appearance of n-type region conductivity at high positive V_{GS} and a slight left shift of the threshold voltage (V_T). Attachment of sfGFP^{204azF} results in a less pronounced conductance decrease (Figure 3c) but a more noticeable left shift of V_T (Figure 3d) corresponding to partial n-doping of scSWCNT, but not the extent to compensate the main charge carriers. A rise in I_{off} is observed for sfGFP^{204azF} because of the reduced channel potential barrier height at lower V_T and the localization of a positively charged protein surface around residue 204 close to the SWCNT (Figure 3f). In comparison, attachment via residue 132 brings a low-density acidic surface charge close to the SWCNT (Figure 3e). Electrostatic doping from the sfGFP surface can affect the charge carrier density in CNTs within the Debye shielding length, which can vary across the surface of a protein. Nevertheless, direct charge transfer can dominate resulting in a decrease of hole charge density and a weak V_T shift. As we state above, attachment via residue 204 brings a positively charged basic surface close to the CNT surface (Figure 3f) that results in an increased electron concentration in the SWCNT so causing a more pronounced left shift of V_T , and a decrease in the total charge carrier concentration. A large increase in resistance was also observed for quasi-metallic nanotubes (qmSWCNT), modified with sfGFP^{204azF} (Figure S5, Supporting Information). As a control, sfGFP containing no phenyl azide groups (i.e., wild-type sfGFP) confirmed the requirement of phenyl azide group for permanent covalent attachment to the SWCNT, as CVCs show only a weak decrease in conductance (Figure S5, Supporting Information); the small conductance drop can be attributed to the effect of UV light on the nanotube and residual weak non-specific adsorption of wild-type GFP.

A relatively wide hysteresis in transfer CVCs (Figure 3b,d) is caused by a number of trapped states near the nanotube channel. The changes in CVCs can be associated with the introduction of sp³ defects and bonds stretching during GFP covalent attachment across a C=C bond, with one protein introducing one defect only. A small number of defects will have less effect on Raman signal change and charge carrier mobility in the carbon nanotube than more extensive modification through chemical coupling with diazonium salts.^[46] Still, the decrease in transconductance after protein attachment is due to the increase of trapped states number in the vicinity of the nanotube surface (Figure 3b,d).

Besides the introduction of additional trapped states, the covalent protein attachment via genetically encoded phenyl azide photochemistry only slightly affects the charge carrier concentration in SWCNT, which is due to the relatively few sfGFP molecules attached using our approach. However, the relatively low number of protein molecules (estimated 1 per 60–80 nm) still leads to a clear wavelength-dependent optoelectronic response with the attachment site determining the conductance characteristics of the whole SWCNT device, as shown hereafter.

2.2. Optoelectronic Effect in sfGFP-SWCNT FETs

FETs like GFP are considered to have inherent light-dependent charge transfer and redox properties^[25,47–52] in addition to their

surface protein electrostatics (vide supra). These properties can, in turn, change carrier density in SWCNT and thus the conductance profile. Through altering the level of the main charge carriers (holes) concentration either negatively (decreasing the number of charges) or positively (increasing the number of charges), conductance can be modulated in the carbon nanotube through local field effects, such as electrostatic doping by the proximal protein surface^[53] or by direct charge transfer.^[3,54] Electrostatic doping has a major initial impact on SWCNT conductance after protein attachment, as discussed above. Direct charge transfer can be developed as a part of GFP function whereby charge transfer on electronic excitation is transduced to the SWCNT.^[30] Optoelectronic control in our devices is likely to occur through the latter process,^[55] where the attachment site of a protein affects the nature and extent of conductance modulation.

We studied the photoresponse of the sfGFP-modified SWCNT transistors by irradiation at different wavelengths (445, 470, and 590 nm). As shown in Figure S1 (Supporting Information), the original wild-type sfGFP and the two azF containing variants free in solution excite and emit to different degrees at the chosen wavelengths (445 and 470 nm), with electronic excitation most efficient at 470 nm (closest to the λ_{max} at 490 nm); there is no electronic excitation or fluorescence emission at 590 nm. Based on the solution spectral properties, we measured the optical response of our SWCNT FETs on irradiation at 470 nm first. SWCNTs modified with one of the two azF containing sfGFP variants show a significant light-dependent conductance decrease on illumination at 470 nm (Figures 4 and S8, Supporting Information). By comparison, only a small increase in conductance is observed on illumination at 470 nm of pristine and wild-type sfGFP (no azF) treated SWCNT transistors (Figures S6 and S7, Supporting Information). For the sfGFP^{132azF}-modified SWCNT device, a 15-fold reduction of conductance occurred within 15.0±1.7 s of illumination (Figure 4a), with no recovery to the initial state on the removal of the light source even after 10 min in the dark. To regenerate the sfGFP^{132azF}-SWCNT FET we applied a gate voltage sweep from –15 to 15 V. After the sweep, illumination of the FET at 470 nm again resulted in a current drop until the next V_{GS} sweep, demonstrating the system can be switched multiple times. For sfGFP^{204azF} modified SWCNT transistors, we also observed an ≈80% drop in current upon 470 nm illumination with a response time of 38.0±1.5 seconds. Unlike sfGFP^{132azF}, total recovery of conductance occurred in the dark within 200 s without applying any V_{GS} sweep. Switching behavior shows good reproducibility over multiple irradiation/dark steps (Figure 4b). The two different protein attachment sites and, hence, molecular configurations result in a different response to light. Thus, we have demonstrated two different and novel bio-optoelectronic effects in SWCNT-based FETs: optical gated transistor (for sfGFP^{204azF}) and optoelectronic memory (for sfGFP^{132azF}). SWCNT-sfGFP^{132azF} FET behaves similarly to the optoelectronic memory device ORAM,^[56] optical switching that is restored under gate voltage sweeping (see, for example, Figure 4a and S8b, Supporting Information). Here one should note that we applied negative $V_{GS} \leq -10$ V during the experiments to work at the operation point in the p-type region because our transistors have negative V_T and I_D close to zero

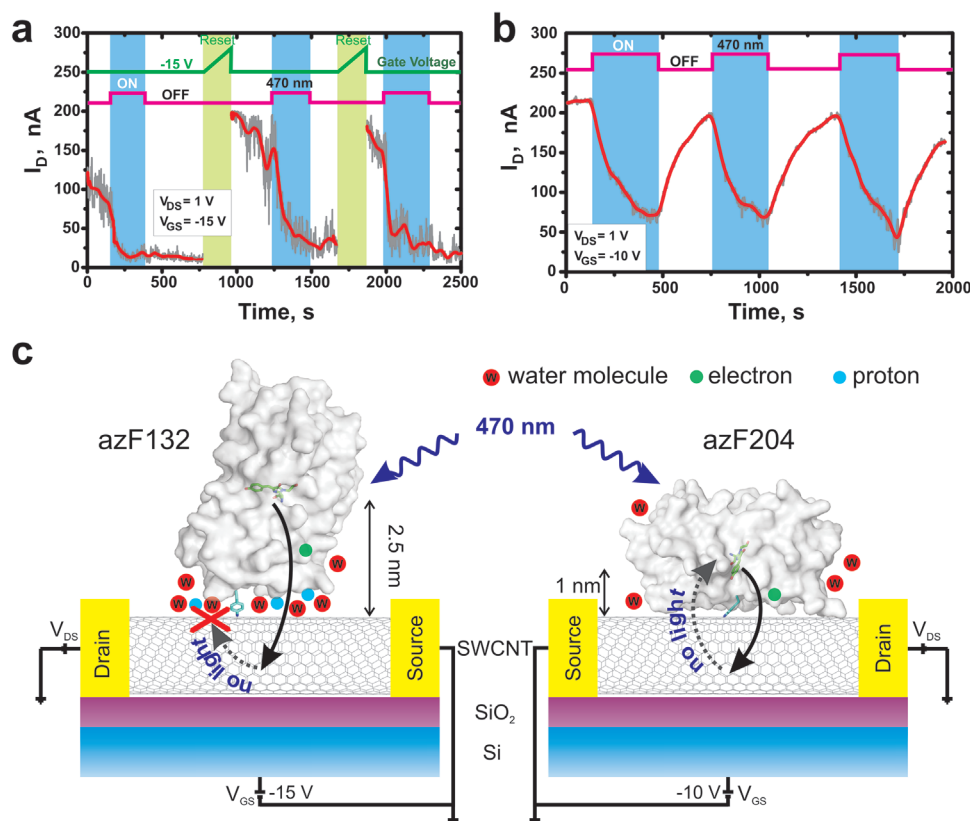


Figure 4. Optical response of fabricated GFP-modified SWCNT transistors. a) Light-induced signal recording with gate voltage-induced dark state recovery in sfGFP^{132azF}-SWCNT FET upon on 470 nm (50 mW cm⁻²) illumination cycling. b) Time course current evolution of the sfGFP^{204azF}-SWCNT FET on 470 nm (50 mW cm⁻²) illumination cycling. c) Two proposed mechanisms of photoinduced electron transfer from the chromophore in sfGFP^{132azF} (left) and sfGFP^{204azF} (right) variants to the SWCNT. Black solid and dotted arrows indicate the pathway of electron transport from the chromophore into SWCNT upon illumination and back under dark, respectively.

for $V_{DS} = 1$ V at $V_{GS} = 0$ V. In this state, the FET channel is fully opened and have the highest conductivity limited only by variations in channel length and contact resistance properties (Figure S9, Supporting Information).

We attribute the optical response of the sfGFP-modified SWCNT transistor to electronic excitation together with the associated charge transfer process and energy emission [fluorescence] and the subsequent return to the ground state (see Figure S1, Supporting Information for spectral features of the variants). For both GFP^{132azF} and GFP^{204azF}, illumination causes a decrease in conductance in p-type sSWCNTs. The likely mechanism for the observed current drop is the electron transfer to the SWCNTs from the photoexcited sfGFP, similar to that previously suggested for GFP bound to graphene, but fabricated via a different chemical attachment process.^[33]

Attachment position with respect to the protein plays a major role in the optoelectronic characteristics of fabricated devices. The chromophore, central to GFP function, is buried within the β -barrel of the protein (Figure 1a) and contributes to an extended polar interaction networks comprising neighboring residues and buried water molecules;^[53,57] these polar interaction networks also contribute to charge transfer pathways.^[25,58] The relative distances of the chromophore from the SWCNT differ between sfGFP^{132azF} (≈ 2.5 nm) and sfGFP^{204azF} (≈ 1 nm). Thus, direct electron tunneling is possible to and from the

nanotube and chromophore attached via both residues.^[59,60] The differences in networks and distances may combine to explain the persistence of the less-conductive state observed for sfGFP^{132azF} compared to sfGFP^{204azF}. Indeed, it has been suggested as a possible explanation for the previously observed difference in fluorescence characteristics on attachment to SWCNTs.^[30] In the case of sfGFP^{132azF}, the prolonged trapping of electrons on water molecules at the protein and nanotube interface (Figure 4c) and water molecules dipole moment rearrangement can result in decreased photo-cycling rates giving rise to dimmer apparent fluorescence and increased resistance to photobleaching observed previously^[30] together with the less conductive state of the SWCNT demonstrated here. Switching the gate voltage causes the relaxation of the dipole moment and drives an electron back to the protein. The closer coupling between the sfGFP chromophore and SWCNT through attachment via residue 204 (Figure 4c) leads to a more efficient charge transfer between the two leading to increased photocycling rates^[30] and recovery of conductance.

It should be noted that the weak modulation of the Schottky barrier height in contact between SWCNT and Au electrode originates under intensive light, even for a pristine nanotube.^[61] Nevertheless, the change in the conductivity of the pristine nanotube (Figure S6, Supporting Information) is an order of magnitude weaker and in the opposite direction than observed for

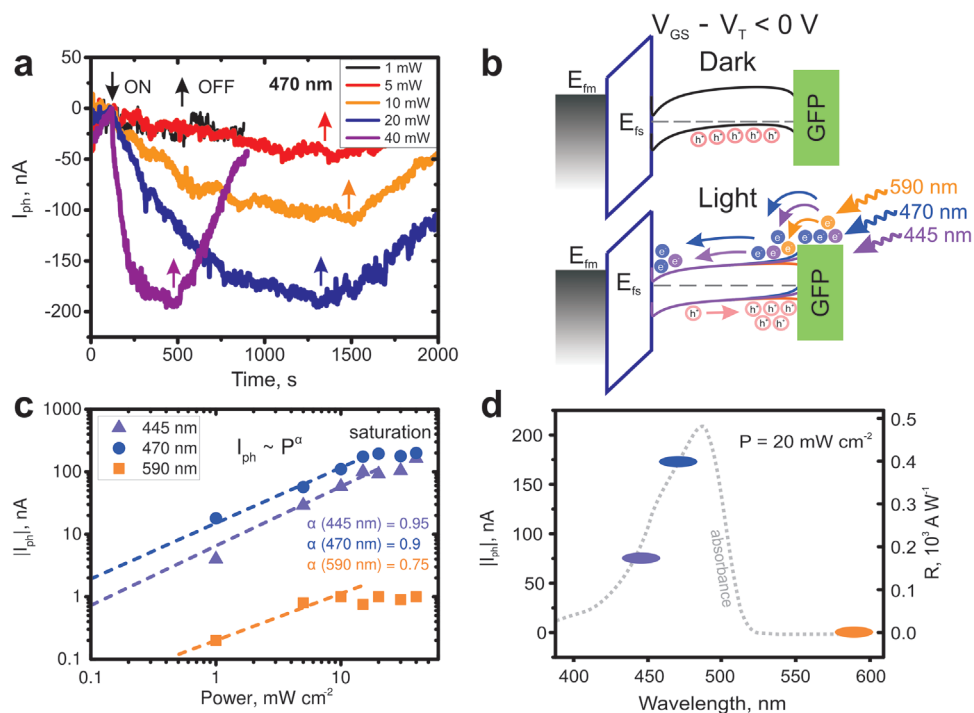


Figure 5. Bio-phototransistor wavelength-specific response. a) Transient photoresponse behavior of SWCNT-sfGFP^{204azF} FET under different power input from the 470 nm LED. b) Energy band diagrams of the phototransistor in the dark (top) and upon light illumination (bottom) at three different wavelengths. c) Nonlinear dependence of current change of irradiation power for different wavelengths. d) I_{ph} and R of phototransistor at different wavelengths. V_{GS} and V_{DS} were set as -10 and 1 V, respectively, during the measurements. The UV-vis absorbance spectra curve of sfGFP^{204azF} is shown as grey dotted lines for comparison.

SWCNT FET modified with azF-containing sfGFP. The changes of output CVCs for both sfGFP^{204azF}- and sfGFP^{132azF}-modified SWCNT FETs upon light irradiation demonstrate a decrease in conductivity with the rise of light intensity (Figure S10, Supporting Information). However, the long integration time during CVC measurements can decrease the effective response.

To further investigate the link between chromophore electronic excitation and nanotube conductance, we exposed the sfGFP^{204azF} SWCNT phototransistors to monochromatic light at different wavelengths and different time points while measuring I_D . The primary electronic excitation determines the optimal wavelength of our device. The wild-type sfGFP and the azF variants have relatively wide absorbance bands spanning from ~ 390 to 500 nm, with a λ_{max} of circa 490 nm. Exposure to 470 nm light generates the biggest response signal for sfGFP^{204azF}-modified SWCNT FET, with power playing a significant role (Figure 5a). A stable photoresponse starts from 1 mW cm⁻², with the saturation observed above 20 mW cm⁻². Specific photoresponses can be explained using energy band diagrams. The barrier at the SWCNT/electrode interface together with SWCNT body affects the SWCNT-FET performance. Here we assume that a channel body effect prevails over the Schottky barrier in fabricated phototransistors. Figure 5b shows the energy band diagram for the scSWCNT phototransistor modified with sfGFP under different illumination conditions, where the bandgap of the individual nanotube (11, 10) was estimated as 0.5 eV. At $V_{GS} \leq -10$ V in the dark, we observe the highest conductivity due to lowering of Schottky barrier and the highest hole concentration in the channel. When illuminated

at the optimal GFP electronic excitation wavelength, the photo-generated electrons in GFP move into the conduction band of scSWCNT, so decreasing the hole concentration. Some of the generated electrons are trapped at the SWCNT/protein and SWCNT/substrate interface. Thus, the light-induced charge transfer from GFP to the SWCNT channel contributes to the current decrease. The optical response is close to linear for 445 and 470 nm illumination before saturation (Figure 5c). It indicates a perfect (close to 100%) light to current conversion due to the low amount of defects in SWCNT after protein attachment.

In optoelectronic devices, photoresponsivity (R) is critical for high-performance photodetectors and signal storage elements development in terms of tuning the conductivity via a specific wavelength. We calculated the maximum responsivity as $R = I_{ph}/P$, where $I_{ph} = |I_{light} - I_{dark}|$ is the current differences with and without light illumination and $P = P_{LED} \times (A_{active}/A_{spot})$,^[62] where P_{LED} is the power of the incident light, A_{active} is the area of a device, and A_{spot} is the spot size of the diode. We choose A_{active} as the device area, which is defined as the distance between source and drain electrodes multiplied by an effective area of nanotube and SiO₂ trapping area (≈ 30 nm).^[43] We found that for the sfGFP^{204azF} SWCNT FET R reaches 0.45×10^3 A W⁻¹ for 470 nm with 20 mW cm⁻² illumination and up to 7×10^3 A W⁻¹ at 470 nm and 1 mW cm⁻². The photoresponse of fabricated devices at different wavelengths correlates well with the absorbance spectrum of sfGFP (Figure 5d). Crucially, it opens up the possibility to detect low-intensity wavelength-specific illumination via the attachment of several different FPs with different λ_{max} to form an array of SWCNT transistors.

As can be seen from the absorbance and fluorescence spectra (Figure S1, Supporting Information), GFP^{204AzF} does not undergo electronic excitation at 590 nm, and this is manifested as a low response for the SWCNT FET on illumination at 590 nm (Figure 5c). GFP^{204AzF} excites at both 445 and 470 nm but interacts with light with different efficiencies, with molar absorbance coefficients ($M^{-1} \text{ cm}^{-1}$) of ≈ 23000 and ≈ 43000 , respectively, and different fluorescence emission intensities. This translates to different responses, with a greater photoresponse observed on illumination at 470 nm compared to 445 nm (Figure 5c,d). Control experiments with pristine SWCNT FETs undergoing the same photochemical attachment procedure but with wild-type sfGFP as the protein show only a small current rise on illumination with 470 nm light (Figure S5a, Supporting Information). Pristine SWCNT FETs not exposed to any protein also resulted in a slight rise in the conductance on illumination with 470 nm light (Figure S6, Supporting Information), which we attribute to a thermoelectric effect in the SWCNT/electrode interface.^[43]

The fastest optical response was observed for 470 nm (Figure S11a, Supporting Information), with increased irradiation power shortening response times (Figures 5a and S11b, Supporting Information). Reducing time of irradiation together with lower light power fits well with the suggested model of trapping states between nanotube and protein. At lower power, the probability of charge transfer is lower. They may be trapped at the interfacial states or return to the chromophore. When the power increases, the probability of charge transfer via tunneling or hopping mechanisms to the nanotube significantly increases, which leads to rapid and high photoresponse to the incident light. To increase the speed of the photogenerated charge carrier separation, one can change the FET channel size either by decreasing the length or by increasing the number of nanotubes in a channel by using a nanotube network.^[63] We have demonstrated that decreasing the channel length of a single SWCNT by about an order of magnitude results in a quicker response time of more than two orders of magnitude (Figure S12, Supporting information). Also, the use of proper substrate material and operating at lower temperatures could increase the response time of SWCNT-based devices.^[64]

Thus, due to the suggested mechanism of site-specific protein attachment to the nanotube, we can control both the number of trapped states and charges at the interfaces using a photoactive protein, which opens up pathways for further design of single-molecule bionanohybrids with tuned functionality.

3. Conclusion

In conclusion, we have demonstrated an optoelectronic biohybrid SWCNT device developed using a simple photochemical attachment process via residue-specific covalent attachment of engineered GFP to sidewalls of individual carbon nanotubes. The covalent functionalization of SWCNTs results in a weak decrease in transconductance, yet highly effective optical performance field-effect transistors. By varying the attachment residue position of GFP, we can change the characteristics of the fabricated device: a phototransistor with the sensitivity of about $7 \times 10^3 \text{ A W}^{-1}$ or optoelectronic memory with rapid photoresponse, low power consumption, 15-fold current modulation, and more than 10 minutes volatile state. Light-induced

direct charge transfer at the sfGFP/SWCNT interface is the likely driver for the optical response with the different protein attachment sites dictating device characteristics. Here we lay the groundwork for GFP-modified SWCNT hybrid sensors with future potential as optically operated memory, fluorescent readout, and molecular transistor devices, as well as eco-friendly interfaces based on photo-activated proteins and electrodes.

4. Experimental Section

Protein Preparation: The engineered GFP variants were produced recombinantly and purified as described previously.^[30,39] All recombinant protein expression was performed in the dark and purification was undertaken in low light conditions.

Fabrication of SWCNT-FET: SWCNT were grown and deposited onto a cold highly doped (p^{++}) 100 mm Si substrate with 300 nm thermal SiO_2 in one process of thermal decomposition of gas-phase ferrocene in the presence of carbon monoxide^[65] with an open reactor. More details on SWCNT-FET development are provided elsewhere.^[43] To achieve the low density of nanotubes, the process was limited to 15 s. The nanotubes are deposited both as an individual nanotube with a diameter of circa 1.5 nm and in bundles. Source and drain 100/15 nm Au/Ti electrodes were fabricated by a photolithographic lift-off process. Highly doped p^{++} Si substrate was used as bottom gate electrode. The distance between source and drain contacts was 12 μm . The substrate was then scribed to isolate devices with a 2 mm^2 area. Further, chips were washed in boiled acetone to delete the photoresist and heated at 250 $^\circ\text{C}$ in a high vacuum to delete the organic residuals. In this work, we studied 10 different FETs with quasi-metallic (4 FETs) or semiconducting nanotubes (6 FETs). The optical images of the devices and SWCNT channel are shown in Figure 2a.

Protein Attachment: Protein attachment was performed as outlined previously.^[30,35] SWCNT-FET chips were rinsed in ethanol and then left to soak for one hour. Then the SWCNT-FET chips were rinsed in distilled H_2O for at least 30–45 s, followed by drying with N_2 gas. During the protein attachment, there was a constant flow of nitrogen over the sample. Protein (100 nM in 25 μl of 50 mM Tris pH 8) sample was cast onto a microchip and irradiated by a 305 nm LED light for 5 minutes. The chip was then rinsed under a fast stream of dH_2O for a minute. Finally, the chip was dried under the nitrogen flow.

Characterization: The optical properties of wild-type GFP, sfGFP^{204AzF} and sfGFP^{132AzF} dialyzed with distilled water were analyzed using a Cary60 UV-Vis spectrophotometer (Agilent, USA) and a Cary Eclipse fluorimeter (Agilent, USA). SWCNT FET samples were characterized via AFM (Solver Pro (NT-MDT, Russia)) using a silicon AFM probe ($f = 140 \text{ kHz}$, $k = 3.5 \text{ N m}^{-1}$, HA_FD/FC Etalon, ScanSense, Germany). The electrical properties of SWCNT transistors were measured by a semiconductor parameter analyzer (IPPP 1/5, MNIPI, Belarus) and a homemade probe station. Raman spectra were carried out on micro-Raman spectrometer Centaur HR (Nanoscan Technology, Russia) with a $\times 100$ objective at 532 nm (Cobolt, Sweden) with a beam spot of $\approx 1 \mu\text{m}^2$ and laser power of 1 mW. Three LEDs (445, 470, and 590 nm) mounted on a fixed holder were used to examine the optoelectronic properties of the phototransistors.

Supporting Information

Supporting Information is available from the Wiley Online Library or from the author.

Acknowledgements

R.E.A.G., N.P.N. and A.V.E. contributed equally to this work. This research was supported by a Russian Science Foundation project no. 19-19-00401 (experiment design, fabrication, characterization of

SWCNT FETs, optical response measurements) and in part by Russian Foundation of Basic Research project no. 20-03-00804 (synthesis of carbon nanotubes). I.B. participated in a project that has received funding from the European Union's Horizon 2020 research and innovation program under grant agreement no. 739570 (ANTARES). D.D.J. would like to thank the EPSRC (EP/J015318/1) for supporting this work. R.E.A.G. (protein preparation, protein attachment) was supported by the Biotechnology and Biological Sciences Research Council-funded South West Biosciences Doctoral Training Partnership [training grant reference BB/M009122/1]. K.R. (protein characterization) was supported by Wellcome Trust Institutional Strategic Support Fund (grant reference AC19101F14). The authors would like to thank the Cardiff School of Biosciences Protein Technology Hub for helping with the production and analysis of proteins.

Conflict of Interest

The authors declare no conflict of interest.

Data Availability Statement

Research data are not shared.

Keywords

bionanohybrids, carbon nanotubes, fluorescent proteins, optoelectronics, phototransistors

Received: December 3, 2021

Revised: January 25, 2022

Published online:

- [1] Q. Ou, B. Yang, J. Zhang, D. Liu, T. Chen, X. Wang, D. Hao, Y. Lu, J. Huang, *Small* **2021**, *17*, 2007241.
- [2] T. Jiang, X. Meng, Z. Zhou, Y. Wu, Z. Tian, Z. Liu, G. Lu, M. Eginlidil, H.-D. Yu, J. Liu, W. Huang, *Nanoscale* **2021**, *13*, 724.
- [3] L. Du, W. Xiong, W. K. Chan, D. L. Phillips, *Nanophotonics* **2020**, *9*, 4689.
- [4] E. A. Rodriguez, R. E. Campbell, J. Y. Lin, M. Z. Lin, A. Miyawaki, A. E. Palmer, X. Shu, J. Zhang, R. Y. Tsien, *Trends Biochem. Sci.* **2017**, *42*, 111.
- [5] R. Y. Tsien, *Annu. Rev. Biochem.* **1998**, *67*, 509.
- [6] N. Karousis, N. Tagmatarchis, D. Tasis, *Chem. Rev.* **2010**, *110*, 5366.
- [7] M. N. Norizan, M. H. Moklis, S. Z. Ngah Demon, N. A. Halim, A. Samsuri, I. S. Mohamad, V. F. Knight, N. Abdullah, *RSC Adv.* **2020**, *10*, 43704.
- [8] V. Georgakilas, M. Otyepka, A. B. Bourlinos, V. Chandra, N. Kim, K. C. Kemp, P. Hobza, R. Zboril, K. S. Kim, *Chem. Rev.* **2012**, *112*, 6156.
- [9] M. Calvaresi, F. Zerbetto, *Acc. Chem. Res.* **2013**, *46*, 2454.
- [10] F. De Leo, A. Magistrato, D. Bonifazi, *Chem. Soc. Rev.* **2015**, *44*, 6916.
- [11] S. Marchesan, M. Prato, *Chem. Commun.* **2015**, *51*, 4347.
- [12] Q. Shao, P. Wu, X. Xu, H. Zhang, C. Cai, *Phys. Chem. Chem. Phys.* **2012**, *14*, 9076.
- [13] P. Jordan, P. Fromme, H. T. Witt, O. Klukas, W. Saenger, N. Krauß, *Nature* **2001**, *411*, 909.
- [14] K. Palczewski, T. Kumasaka, T. Hori, C. A. Behnke, H. Motoshima, B. A. Fox, I. Le Trong, D. C. Teller, T. Okada, R. E. Stenkamp, M. Yamamoto, *Science* **2000**, *289*, 739.
- [15] F. Arnesano, L. Banci, I. Bertini, J. Faraone-Mennella, A. Rosato, P. D. Barker, A. R. Fersht, *Biochemistry* **1999**, *38*, 8657.
- [16] D. Nishiori, W. Zhu, R. Salles, M. Miyachi, Y. Yamanoi, T. Ikuta, K. Maehashi, T. Tomo, H. Nishihara, *ACS Appl. Mater. Interfaces* **2019**, *11*, 42773.
- [17] J. M. Artés, I. Díez-Pérez, P. Gorostiza, *Nano Lett.* **2012**, *12*, 2679.
- [18] E. A. Della Pia, Q. Chi, J. E. Macdonald, J. Ulstrup, D. D. Jones, M. Elliott, *Nanoscale* **2012**, *4*, 7106.
- [19] E. A. Della Pia, Q. Chi, D. D. Jones, J. E. Macdonald, J. Ulstrup, M. Elliott, *Nano Lett.* **2011**, *11*, 176.
- [20] M. Zimmer, *Chem. Soc. Rev.* **2009**, *38*, 2823.
- [21] J. M. Zajac, M. Schubert, T. Roland, C. Keum, I. D. W. Samuel, M. C. Gather, *Adv. Funct. Mater.* **2018**, *28*, 1706300.
- [22] V. Fernández-Luna, P. B. Coto, R. D. Costa, *Angew. Chem., Int. Ed.* **2018**, *57*, 8826.
- [23] M. C. Gather, S. H. Yun, *Nat. Commun.* **2014**, *5*, 5722.
- [24] K. V. Korpany, P. Langat, D. M. Kim, N. Edelman, D. R. Cooper, J. Nadeau, A. S. Blum, *J. Am. Chem. Soc.* **2012**, *134*, 16119.
- [25] A. Acharya, A. M. Bogdanov, B. L. Grigorenko, K. B. Bravaya, A. V. Nemukhin, K. A. Lukyanov, A. I. Krylov, *Chem. Rev.* **2017**, *117*, 758.
- [26] A. M. Bogdanov, A. S. Mishin, I. V. Yampolsky, V. V. Belousov, D. M. Chudakov, F. V. Subach, V. V. Verkhusha, S. Lukyanov, K. A. Lukyanov, *Nat. Chem. Biol.* **2009**, *5*, 459.
- [27] S. Ghasemi, K. Moth-Poulsen, *Nanoscale* **2021**, *13*, 659.
- [28] M. Freeley, H. L. Worthy, R. Ahmed, B. Bowen, D. Watkins, J. E. Macdonald, M. Zheng, D. D. Jones, M. Palma, *J. Am. Chem. Soc.* **2017**, *139*, 17834.
- [29] Q. H. Wang, Z. Jin, K. K. Kim, A. J. Hilmer, G. L. C. Paulus, C.-J. Shih, M.-H. Ham, J. D. Sanchez-Yamagishi, K. Watanabe, T. Taniguchi, J. Kong, P. Jarillo-Herrero, M. S. Strano, *Nat. Chem.* **2012**, *4*, 724.
- [30] S. K. Thomas, W. D. Jamieson, R. E. A. Gwyther, B. J. Bowen, A. Beachey, H. L. Worthy, J. E. Macdonald, M. Elliott, O. K. Castell, D. D. Jones, *Bioconjugate Chem.* **2020**, *31*, 584.
- [31] J. Tong, L. Zhang, Y. Wang, T. Li, *Front. Mater.* **2020**, *7*.
- [32] V. Bakaraju, E. S. Prasad, B. Meena, H. Chaturvedi, *ACS Omega* **2020**, *5*, 9702.
- [33] Y. Lu, M. B. Lerner, Z. John Qi, J. J. Mitala, J. Hsien Lim, B. M. Discher, A. T. Charlie Johnson, *Appl. Phys. Lett.* **2012**, *100*, 033110.
- [34] J.-D. Pédelacq, S. Cabantous, T. Tran, T. C. Terwilliger, G. S. Waldo, *Nat. Biotechnol.* **2006**, *24*, 79.
- [35] A. J. Zaki, A. M. Hartley, S. C. Reddington, S. K. Thomas, P. Watson, A. Hayes, A. V. Moskalenko, M. F. Craciun, J. E. Macdonald, D. D. Jones, M. Elliott, *RSC Adv.* **2018**, *8*, 5768.
- [36] J. W. Chin, S. W. Santoro, A. B. Martin, D. S. King, L. Wang, P. G. Schultz, *J. Am. Chem. Soc.* **2002**, *124*, 9026.
- [37] S. Reddington, P. Watson, P. Rizkallah, E. Tippmann, D. D. Jones, *Biochem. Soc. Trans.* **2013**, *41*, 1177.
- [38] S. C. Reddington, P. J. Rizkallah, P. D. Watson, R. Pearson, E. M. Tippmann, D. D. Jones, *Angew. Chem., Int. Ed.* **2013**, *52*, 5974.
- [39] S. C. Reddington, E. M. Tippmann, D. D. Jones, *Chem. Commun.* **2012**, *48*, 8419.
- [40] D. Satco, A. R. T. Nugraha, M. S. Ukhtary, D. Kopylova, A. G. Nasibulin, R. Saito, *Phys. Rev. B* **2019**, *99*, 075403.
- [41] J. López-Andarías, S. H. Mejías, T. Sakurai, W. Matsuda, S. Seki, F. Feixas, S. Osuna, C. Atienza, N. Martín, A. L. Cortajarena, *Adv. Funct. Mater.* **2018**, *28*, 1704031.
- [42] P. P. Pal, T. Larionova, I. V. Anoshkin, H. Jiang, M. Nisula, A. A. Goryunkov, O. V. Tolochko, M. Karppinen, E. I. Kauppinen, A. G. Nasibulin, *J. Phys. Chem. C* **2015**, *119*, 27821.
- [43] A. V. Emelianov, N. P. Nekrasov, M. V. Moskotin, G. E. Fedorov, N. Otero, P. M. Romero, V. K. Nevolin, B. I. Afanogenov, A. G. Nasibulin, I. I. Bobrinetskiy, *Adv. Electron. Mater.* **2021**, *7*, 2000872.
- [44] S. Santos, V. Barcons, H. K. Christenson, J. Font, N. H. Thomson, *PLoS One* **2011**, *6*, e23821.
- [45] M. E. Fuentes-Perez, M. S. Dillingham, F. Moreno-Herrero, *Methods* **2013**, *60*, 113.

- [46] M. B. Lerner, J. D'Souza, T. Pazina, J. Dailey, B. R. Goldsmith, M. K. Robinson, A. T. C. Johnson, *ACS Nano* **2012**, *6*, 5143.
- [47] T. Sen, Y. Ma, I. V. Polyakov, B. L. Grigorenko, A. V. Nemukhin, A. I. Krylov, *J. Phys. Chem. B* **2021**, *125*, 757.
- [48] L. Tang, Y. Wang, L. Zhu, K. Kallio, S. J. Remington, C. Fang, *Phys. Chem. Chem. Phys.* **2018**, *20*, 12517.
- [49] D. Stoner-Ma, A. A. Jaye, K. L. Ronayne, J. Nappa, S. R. Meech, P. J. Tonge, *J. Am. Chem. Soc.* **2008**, *130*, 1227.
- [50] X. Lv, Y. Yu, M. Zhou, C. Hu, F. Gao, J. Li, X. Liu, K. Deng, P. Zheng, W. Gong, A. Xia, J. Wang, *J. Am. Chem. Soc.* **2015**, *137*, 7270.
- [51] L. M. Oltrogge, Q. Wang, S. G. Boxer, *Biochemistry* **2014**, *53*, 5947.
- [52] J. J. van Thor, *Chem. Soc. Rev.* **2009**, *38*, 2935.
- [53] K. Brejc, T. K. Sixma, P. A. Kitts, S. R. Kain, R. Y. Tsien, M. Ormo, S. J. Remington, *Proc. Natl. Acad. Sci. U.S.A.* **1997**, *94*, 2306.
- [54] K. Bradley, M. Briman, A. Star, G. Grüner, *Nano Lett.* **2004**, *4*, 253.
- [55] S. Yoo, D. S. Kim, W.-K. Hong, J. Il Yoo, F. Huang, H. C. Ko, J. H. Park, J. Yoon, *ACS Appl. Mater. Interfaces* **2021**, acsami.1c15565.
- [56] F. Zhou, J. Chen, X. Tao, X. Wang, Y. Chai, *Research* **2019**, *2019*, 9490413.
- [57] O. V. Stepanenko, V. V. Verkhusha, M. M. Shavlovsky, I. M. Kuznetsova, V. N. Uversky, K. K. Turoverov, *Proteins: Struct., Funct., Bioinf.* **2008**, *73*, 539.
- [58] A. Shinobu, G. J. Palm, A. J. Schierbeek, N. Agmon, *J. Am. Chem. Soc.* **2010**, *132*, 11093.
- [59] A. A. Stuchebrukhov, *Laser Phys.* **2010**, *20*, 125.
- [60] J. R. Winkler, H. B. Gray, *J. Am. Chem. Soc.* **2014**, *136*, 2930.
- [61] P. Avouris, M. Freitag, V. Perebeinos, *Nat. Photonics* **2008**, *2*, 341.
- [62] V. T. Nguyen, W. Yim, S. J. Park, B. H. Son, Y. C. Kim, T. T. Cao, Y. Sim, Y.-J. Moon, V. C. Nguyen, M.-J. Seong, S.-K. Kim, Y. H. Ahn, S. Lee, J.-Y. Park, *Adv. Funct. Mater.* **2018**, *28*, 1802572.
- [63] X. He, F. Léonard, J. Kono, *Adv. Opt. Mater.* **2015**, *3*, 989.
- [64] G. Fedorov, A. Kardakova, I. Gayduchenko, I. Charayev, B. M. Voronov, M. Finkel, T. M. Klapwijk, S. Morozov, M. Presniakov, I. Bobrinetskiy, R. Ibragimov, G. Goltsman, *Appl. Phys. Lett.* **2013**, *103*, 181121.
- [65] A. Moiala, A. G. Nasibulin, D. P. Brown, H. Jiang, L. Khriachtchev, E. I. Kauppinen, *Chem. Eng. Sci.* **2006**, *61*, 4393.